Monthly Notices
of the
ROYAL ASTRONOMICAL SOCIETY

Mon. Not. R. Astron. Soc. **421,** 3481–3487 (2012) doi:10.1111/j.1365-2966.2012.20573.x

Haloes and voids in $f(R)$ gravity

Baojiu Li,[1,2,3,4]★ Gong-Bo Zhao[5]★ and Kazuya Koyama[5]★

[1]*Institute for Computational Cosmology, Department of Physics, University of Durham, South Road, Durham DH1 3LE*
[2]*DAMTP, Centre for Mathematical Sciences, University of Cambridge, Wilberforce Road, Cambridge CB3 0WA*
[3]*Kavli Institute for Cosmology Cambridge, Madingley Road, Cambridge CB3 0HA*
[4]*Institute of Astronomy, Madingley Road, Cambridge CB3 0HA*
[5]*Institute of Cosmology and Gravitation, University of Portsmouth, Dennis Sciama Building, Portsmouth PO1 3FX*

Accepted 2012 January 15. Received 2011 December 20; in original form 2011 November 23

ABSTRACT

In this paper, we study the distribution of dark matter haloes and voids using high-resolution simulations in $f(R)$ gravity models with the chameleon mechanism to screen the fifth force in a dense environment. For dark matter haloes, we show that the semi-analytic thin-shell condition provides a good approximation to describe the mass and environmental dependence of the screening of the fifth force in haloes. Due to stronger gravity, there are far more massive haloes and large voids in $f(R)$ models compared with Λ cold dark matter (ΛCDM) models. The numbers of voids with an effective radius of $15\,h^{-1}$ Mpc are twice and four times as many as those in ΛCDM for $f(R)$ models with $|f_{R0}| = 10^{-5}$ and 10^{-4}, respectively. This provides a new means to test the models using the upcoming observational data. We also find that haloes inside voids are significantly less screened in our simulations, and so are ideal objects for the gravity test.

Key words: methods: analytical – methods: numerical – cosmology: theory – dark energy – large-scale structure of Universe.

1 INTRODUCTION

The biggest problem in cosmology is to explain the observed accelerated expansion of the Universe. Within the framework of general relativity (GR), the acceleration originates from dark energy (Copeland, Sami & Tsujikawa 2006). Alternatively, a large-distance modification to GR may account for the late-time acceleration of the Universe.

It has been recognized that usually once we modify Einstein gravity on large scales, there can appear a new scalar degree of freedom in gravity which mediates a fifth force. Without a mechanism to suppress this additional force, most modified gravity models are excluded by stringent constraints on deviations from GR on the Solar system scale. One way to evade these constraints is to exploit a chameleon mechanism (Khoury & Weltman 2004; Mota & Shaw 2007). The new scalar degree of freedom couples to the energy density of matter. By tuning the coupling and potential for the scalar mode, it is possible to realize a situation that in dense environments such as the Solar system, the scalar field has a large mass and it essentially does not mediate the fifth force. On the other hand, on cosmological scales, this scalar mode is light and modifies gravity significantly.

In models with the chameleon mechanism, there appears an environmental dependence on the properties of dark matter distributions. In dense environments such as clusters, the chameleon works efficiently and the modification of gravity is suppressed. On the other hand, in underdense regions such as voids, the chameleon mechanism does not work and gravity is significantly modified. As is shown in our previous paper (Zhao, Li & Koyama 2011b), this environmental dependence is a smoking gun for the modification of gravity in models with the chameleon mechanism.

In this paper, we study the properties of dark matter haloes and voids in models with the chameleon mechanism to reveal the environmental dependence of dark matter distributions. We use $f(R)$ gravity (Carroll et al. 2005) as an example and exploit recent results from high-resolution simulations described in Zhao, Li & Koyama (2011a). In the $f(R)$ gravity, the fifth force can enhance gravity by a factor of 1/3, but this enhancement is suppressed by the chameleon mechanism in the overdense regions. Some other numerical simulations performed for models with the chameleon mechanism are those in Oyaizu (2008), Oyaizu, Lima & Hu (2008), Schmidt et al. (2008), Li & Zhao (2009, 2010), Zhao et al. (2010) and Li et al. (2012). Simulations for models that suppress the fifth force using other mechanisms (Brax et al. 2010; Hinterbichler & Khoury 2010) have also been done (Brax et al. 2011; Davis et al. 2011). Although we will not study those simulations directly, we expect that the results found here will be true for them as well.

The paper is organized as follows. In Section 2, we summarize $f(R)$ gravity models that we shall study in this paper. In Section 3, we study the probability distribution function of the smoothed density field and show how the properties of haloes and voids in $f(R)$ gravity

★E-mail: baojiu.li@durham.ac.uk (BL); gong-bo.zhao@port.ac.uk (G-BZ); kazuya.koyama@port.ac.uk (KK)

are modified compared with the standard ΛCDM model. Section 4 is devoted to the study of dark matter haloes. We study how the difference between dynamical and lensing masses, which arises due to the fifth force, depends on the mass and environment of haloes. We find that the semi-analytic thin-shell condition that determines the efficiency of the chameleon can well describe those dependences found in simulations. In Section 5, we study the underdense regions by identifying voids in our simulations. We study the properties of haloes inside and near the voids. We show that the number density of large voids is significantly modified in $f(R)$ gravity models.

2 $f(R)$ GRAVITY AND SIMULATIONS

The $f(R)$ gravity, in which the Ricci scalar R in the Einstein–Hilbert action is generalized to a function of R, was designed to explain the observed cosmic acceleration without introducing dark energy. In such theories, the structure formation is determined by the following equations:

$$\nabla^2\Phi = \frac{16\pi G}{3}a^2\delta\rho_{\rm M} + \frac{a^2}{6}\delta R(f_R), \tag{1}$$

$$\nabla^2\delta f_R = -\frac{a^2}{3}[\delta R(f_R) + 8\pi G\delta\rho_{\rm M}], \tag{2}$$

where Φ denotes the gravitational potential, $f_R \equiv {\rm d}f(R)/{\rm d}R$ is the *scalaron*, the extra scalar degree of freedom, $\delta R = R - \bar{R}$, $\delta\rho_{\rm M} = \rho_{\rm M} - \bar{\rho_{\rm M}}$ and the quantities with overbar take the background values. In GR, the gravitational potential is solely determined by the distribution of matter, say, $\nabla^2\Phi = 4\pi G a^2\delta\rho_{\rm M}$. This is a linear Poisson equation, which is much easier to solve. In $f(R)$, however, the scalar field complicates the Poisson equation, making the effective Newton's constant vary with the local density: in underdense regions, the $\delta R(f_R)$ term in equation (1) vanishes; thus two equations decouple, making the effective Newton's constant enhanced by 1/3. On the other hand, in the dense region, δf_R in equation (2) is negligible, so $\delta R(f_R) = -8\pi G\delta\rho_{\rm M}$, which means that GR is locally restored. This is the chameleon mechanism making $f(R)$ evade the stringent Solar system tests and thus is important for the cosmological viability of the $f(R)$ gravity.

One could rewrite equation (1) as

$$\nabla^2\Phi = 4\pi G a^2\delta\rho_{\rm eff}, \tag{3}$$

where the effect of the scalar field is absorbed into the definition of the effective energy density $\delta\rho_{\rm eff}$. Then the dynamical mass $M_{\rm D}(r)$ of a halo is defined as the mass contained within a radius r, inferred from the gravitational potential felt by a test particle at r. It is given by $M_{\rm D} \equiv \int a^2\delta\rho_{\rm eff}{\rm d}V$, in which the integral is over the extension of the body. On the other hand, the lensing mass is the true mass of the halo, i.e. $M_{\rm L} \equiv \int a^2\delta\rho_{\rm M}{\rm d}V$.

Comparing the lensing mass with the dynamical mass of the same halo can in principle be an easy way to test GR. This is because the lensing mass and the dynamical mass are identical in GR, but quite different in modified gravity scenarios. To quantify the difference, we calculate the relative difference Δ_M between $M_{\rm L}$ and $M_{\rm D}$ for each halo, $\Delta_M \equiv M_{\rm D}/M_{\rm L} - 1$. Note that in $f(R)$, $\Delta_M \leq 1/3$ (Zhao, Li & Koyama 2011b).

The presence of the chameleon effect indicates that equations (1) and (2) are highly non-linear, so that the system cannot be solved without using N-body simulations. In this work, we shall use the high-resolution N-body simulation catalogue (Zhao et al. 2011a) for an $f(R)$ gravity model, $f(R) = \alpha R/(\beta R + \gamma)$ (Hu & Sawicki 2007), where $\alpha = -m^2c_1$, $\beta = c_2$, $\gamma = -m^2$, $m^2 = H_0^2\Omega_{\rm M}$ and c_1, c_2 are free parameters. The expansion rate of the universe in this $f(R)$ model is determined by c_1/c_2, and the structure formation depends on $|f_{R0}|$, which is the value of $|{\rm d}f/{\rm d}R|$ at $z = 0$, and is proportional to c_1/c_2^2. We tune c_1/c_2 to obtain the same expansion history as that in a ΛCDM model and choose values for $|f_{R0}|$ so that those models cannot be ruled out by current Solar system tests. To satisfy these requirements, we set $c_1/c_2 = 6\Omega_\Lambda/\Omega_{\rm M}$ and simulate three models with $|f_{R0}| = 10^{-4}, 10^{-5}$ and 10^{-6}. In this paper, we study the distribution of dark matter haloes and voids in these simulations at $z = 0$. The method to identify haloes is described in Li & Barrow (2011) and Zhao et al. (2011a).

3 PROBABILITY DISTRIBUTION OF DENSITY FIELD

In the standard CDM paradigm, structures grow from the small inhomogeneities in the initial matter density field due to the pull of

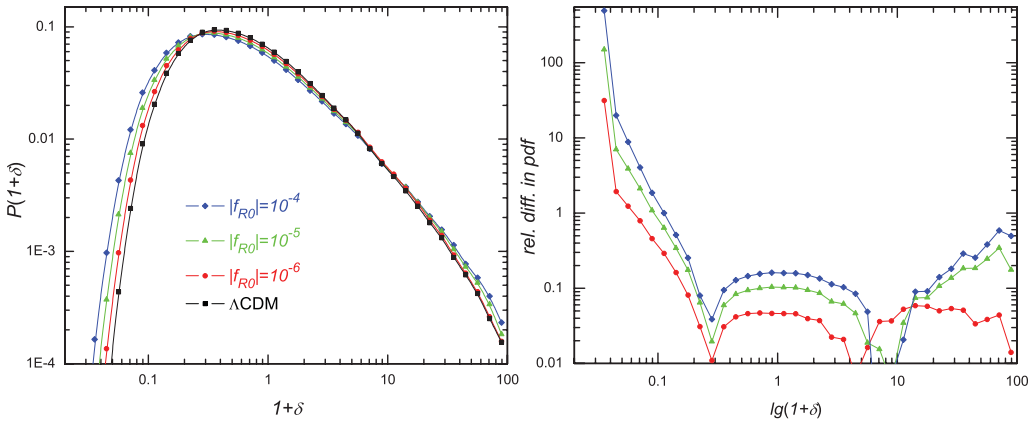

Figure 1. Left-hand panel: the probability distribution of the matter density contrast field $\delta \equiv \rho(\boldsymbol{x}; R)/\bar{\rho} - 1$. The δ field was filtered by a top-hat window with radius $R = 2\,h^{-1}$ Mpc. In the plot, we offset δ by 1 to use the logarithmic scale and the points plotted homogeneously in $\log(1 + \delta)$. The black squares, red circles, green triangles and blue diamonds are from the ΛCDM simulation and $f(R)$ simulations with $|f_{R0}| = 10^{-6}, 10^{-5}, 10^{-4}$, respectively. Each curve represents the averaged result over 10 realizations and is normalized so that the integration of $P(1 + \delta)$ is 1. Right-hand panel: the relative differences of $|P(1 + \delta)|$ in $f(R)$ and ΛCDM models. The symbols are the same as in the left-hand panel, but this shows more clearly that the $f(R)$ model is much more efficient in evacuating low-density regions.

gravity. As a result, initial overdense (underdense) regions become more and more overdense (underdense). In $f(R)$ gravity, gravity can be enhanced, so that the fifth force helps us to pull more matter into overdense regions and the underdense regions can be evacuated more efficiently.

In Fig. 1 we show the probability distribution of the matter density contrast field measured from our $f(R)$ and ΛCDM simulations. This is calculated by filtering the density field by top-hat windows with, for example, radius $R = 2\,h^{-1}$ Mpc centred at each cell of the simulation grid and by counting how many such windows fall into a given density band.

As shown in this figure, the fifth force can tremendously increase the chance of creating extremely low-density regions in the Universe. For example, only ∼0.01 per cent of the space in the ΛCDM paradigm has a density of $1 + \delta = 0.05$, while the $f(R)$ models predict five (for $|f_{R0}| = 10^{-6}$), 15 (for $|f_{R0}| = 10^{-5}$) and 30 (for $|f_{R0}| = 10^{-4}$) times as much. The effect becomes smaller for increasing δ, and for $1 + \delta \sim 0.2$–0.3 the probability becomes roughly the same for all models. For $0.2\text{–}0.3 < 1 + \delta \lesssim 10$, the fifth force actually decreases the probability, and then for windows with $1 + \delta > \sim 10$, the fifth force makes it more likely to be found again by making matter cluster more strongly. Similar effects have been found for other models (Hellwing & Juszkiewicz 2009; Li 2011).

The peak of the density distribution shifts towards low values as $|f_{R0}|$ increases, which shows that the Universe in $f(R)$ gravity may look emptier overall. Meanwhile, Fig. 1 confirms that an $f(R)$ universe will more likely host very big voids and very massive dark matter haloes, both of which are rarer in a ΛCDM universe. We will come back to this point later.

Fig. 1 also clearly shows the effect of the chameleon mechanism, which is known to work better for smaller $|f_{R0}|$ and for high-density fields (Zhao et al. 2011a). For $|f_{R0}| = 10^{-6}$, the deviation from ΛCDM is suppressed for high-density fields, while there is still a sizable deviation in the probability distribution for underdense fields. This shows that the modification of gravity is more prominent for voids for small $|f_{R0}|$. This fact is important when we perform observational tests of modified gravity models with a realistic value of $|f_{R0}|$ compatible with the Solar system constraints.

4 OVERDENSE REGIONS

In general, dark matter haloes reside in high-density regions, which form their local environment. It is well known that the fifth force in $f(R)$ gravity sensitively depends on the environment. Thus from a theoretical point of view, it is very important to understand how the environment changes the properties of the fifth force.

As mentioned above, $f(R)$ gravity is a subclass of the chameleon scalar field theory, with $f_R = \exp(\gamma\sqrt{\kappa}\varphi) - 1$, where $\kappa = 8\pi G = M_{\rm Pl}^{-2}$ and φ is the corresponding scalar field and $\gamma = \sqrt{2/3}$ is the constant coupling strength. The scalar field is governed by an effective potential (see e.g. Li & Barrow 2007)

$$V_{\rm eff}(\varphi) = \frac{Rf_R - f}{2\kappa\,(1 + f_R)^2} + \frac{1}{4}\rho_{\rm m}\exp\left(\gamma\sqrt{\kappa}\varphi\right). \quad (4)$$

When the chameleon mechanism is at work, a spherical body will develop a thin shell, the thickness of which is given by (Khoury & Weltman 2004; Li & Efstathiou 2011)

$$\frac{\Delta R}{R} = \frac{\varphi_{\rm out} - \varphi_{\rm in}}{\gamma\sqrt{\kappa}\rho_{\rm in}R^2}, \quad (5)$$

where R is the radius of the body, ΔR is the thickness of the shell, $\varphi_{\rm out}$, $\varphi_{\rm in}$ are the values of φ minimizing $V_{\rm eff}$ inside and outside the body, respectively. Similarly, $\rho_{\rm in}$ and $\rho_{\rm out}$ are the constant matter density inside and outside the body, respectively. Note that only the matter within the thin shell contributes to the fifth force exerted on a nearby test particle. From equation (5), it is evident that the fifth force could be suppressed if shell becomes thinner, which can be realized in the following two ways:

(i) increasing R and/or $\rho_{\rm in}$, thereby making the body (in the case here the dark matter halo) more massive;

(ii) decreasing $\varphi_{\rm out}$, which involves increasing $\rho_{\rm out}$ or equivalently making the environment denser.[1]

As a result, massive haloes in dense environments are strongly screened from the fifth force, while small haloes in low-density environments are less screened and may experience the full fifth force.

In the $f(R)$ gravity theory, the thin-shell expression (equation 5) can be translated into the equation

$$\frac{\Delta R}{R} \approx \frac{f_{R,\rm in} - f_{R,\rm out}}{\gamma^2\kappa\rho_{\rm in}R^2} \quad (6)$$

by using the relationship between $\sqrt{\kappa}\varphi$ and f_R and the fact that $\sqrt{\kappa}\varphi \sim |f_R| \ll 1$. The ratio between the magnitudes of the fifth force and gravity can be approximately estimated as (Li & Efstathiou 2011)

$$\Delta_M = \frac{\gamma^2}{2} \times \min\left\{\frac{3\Delta R}{R}, 1\right\} = \frac{1}{3} \times \min\left\{\frac{3\Delta R}{R}, 1\right\}. \quad (7)$$

Δ_M has a maximum value of 1/3 as expected, and it can be analytically estimated by calculating $\Delta R/R$ from equation (6) as follows.

(i) Given a halo's mass and virial radius, we can compute the average $\rho_{\rm in}$ and therefore $f_{R,\rm in}$.

(ii) $\rho_{\rm out}$, the environmental density, can be estimated by computing the average density of a sphere with a radius $R_{\rm env}$ centring on the concerned halo (Li & Efstathiou 2011). Then $f_{R,\rm out}$ follows straightforwardly.

As mentioned above, $\varphi_{\rm in}$, $\varphi_{\rm out}$ (or equivalently $f_{R,\rm in}$, $f_{R,\rm out}$) are obtained by minimizing the effective potential $V_{\rm eff}$ or its $f(R)$-gravity counterpart (Khoury & Weltman 2004), which is essentially solving the equation $R(f_R) = 8\pi G\rho_{\rm m}$, which does not hold in the $f(R)$ gravity in general. It can nevertheless be used here because (1) $f_{R,\rm out}$ is solved by assuming a homogeneous background on which $\nabla^2 f_R = 0$ (cf. equation 2), and (2) if there exists a thin shell, then somewhere inside the halo we do have $R = 8\pi G\rho_{\rm m}$ (Hu & Sawicki 2007) – which means $f_{R,\rm in}$ minimizes $V_{\rm eff}$ there.[2] For the models considered here, we have

$$f_{R,\rm in} = \frac{\left(1 + 4\frac{\Omega_\Lambda}{\Omega_{\rm m}}\right)^2}{\left(\tilde{\rho}_{\rm in} + 4\frac{\Omega_\Lambda}{\Omega_{\rm m}}\right)^2} f_{R0}, \quad (8)$$

[1] Note that the first term on the right-hand side of equation (4) is a runaway potential of φ, while the second term increases exponentially in φ. Therefore, $V_{\rm eff}(\varphi)$ has a global minimum, which shifts towards smaller values of φ when $\rho_{\rm m}$ increases.

[2] Ideally, $f_{R,\rm in}$ would be the true value of f_R in the halo, which is not necessarily equal to our analytical approximation or even a constant, but unfortunately there is no analytical formula for this. None the less, using the above estimate of $f_{R,\rm in}$ in the thin-shell condition does, as we shall see below, give reasonable results.

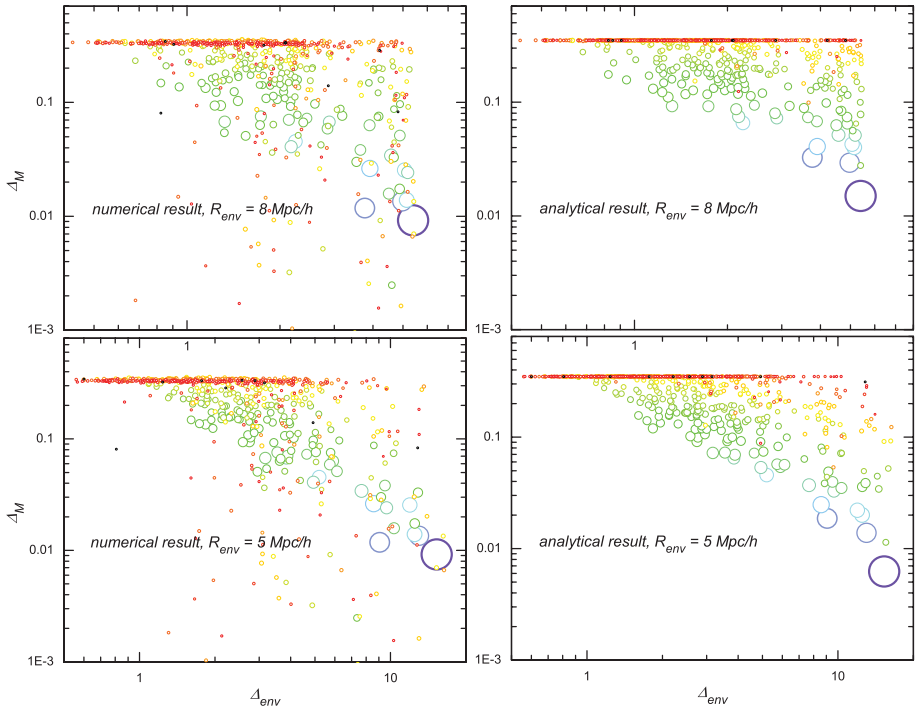

Figure 2. Screening of dark matter haloes as a function of the environment and halo mass for the model with $|f_{R0}| = 10^{-6}$. The horizontal axis is $\Delta_{\rm env}$, the matter overdensity of a sphere (the environment) centred at each halo, with comoving radius $R_{\rm env}$ as indicated in the panels. The vertical axis is Δ_M, the ratio between the magnitudes of the fifth force and gravity at the surface of a halo. Each circle represents a halo, and the halo's mass is illustrated by both the size (increasing size for increasing mass) and colour (from red to violet for increasing mass) of the circle. The left-hand (right-hand) panels are numerical (analytical) results (see text for a detailed description).

$$f_{R,\rm out} = \frac{\left(1+4\frac{\Omega_\Lambda}{\Omega_{\rm m}}\right)^2}{\left(\tilde{\rho}_{\rm out}+4\frac{\Omega_\Lambda}{\Omega_{\rm m}}\right)^2} f_{R0}, \tag{9}$$

at $z = 0$, where $\tilde{\rho}_{\rm out(in)} \equiv \rho_{\rm out(in)}/\bar{\rho}$. Therefore, we get Δ_M from equation (7), with

$$\frac{\Delta R}{R} \approx \frac{\left(1+4\frac{\Omega_\Lambda}{\Omega_{\rm m}}\right)^2}{2\tilde{\rho}_{\rm in}\Omega_{\rm m}(RH_0)^2}|f_{R0}| \times \left[\frac{1}{\left(\tilde{\rho}_{\rm out}+4\frac{\Omega_\Lambda}{\Omega_{\rm m}}\right)^2} - \frac{1}{\left(\tilde{\rho}_{\rm in}+4\frac{\Omega_\Lambda}{\Omega_{\rm m}}\right)^2}\right]. \tag{10}$$

This could be measured for each halo from the N-body simulations, as is shown in Fig. 2. The thin-shell condition for dark matter haloes has been derived in Khoury & Weltman (2004) and Hu & Sawicki (2007) and studied using N-body simulations by Schmidt (2010), but here for the first time we have checked the environmental effects and compared with analytical results.

The left-hand panels of Fig. 2 show the dependence of Δ_M on the halo mass (illustrated by the size and colour of the symbols) and the environment matter density (horizontal axis). The results are measured from our N-body simulations using two values of $R_{\rm env}$: $8\,h^{-1}$ Mpc (upper-left panel) and $5\,h^{-1}$ Mpc (lower-left panel). There are several interesting features.

(i) Massive haloes mostly reside in overdense regions, as could be seen from the correlation between the size of the symbols and the horizontal axis. This is as expected, because only in those regions are there enough particles to form large haloes.

(ii) With the same environmental density, small haloes are less screened (have bigger Δ_M), which agrees with the analysis above.

(iii) For haloes with comparable mass, those in overdense regions are more strongly screened, because of the environmental effect.

(iv) Only very few haloes reside in underdense regions, and those are mostly small haloes. This is because most particles in those regions have been pulled away. Note that the haloes in those regions are essentially unscreened.

(v) The dependence of the results on $R_{\rm env}$ is fairly weak, indicating that the exact value of $R_{\rm env}$ in the definition of the environment is not crucial.

In the right-hand panels of Fig. 2, we have shown the analytical approximation obtained by using equation (10). We can find that the analytical result agrees with the N-body simulation result quite well, and once again there is no sensitive dependence on $R_{\rm env}$. This means that the analytical approximation (10) can well describe the non-linear behaviour of the fifth force in $f(R)$ gravity.

In Fig. 3 we show the same results for a different $f(R)$ model, with $|f_{R0}| = 10^{-5}$. Again we could see that the analytical and numerical results agree well. Note that here all haloes but the very massive ones are unscreened. Figs 2 and 3 lend support to the simple excursion-set model of Li & Efstathiou (2011) for studying structure formation in the chameleon-type scalar field models.

Of course, the agreement between the analytical and simulation results is not perfect, although it is fairly good statistically. For $|f_{R0}| = 10^{-5}$, the analytic thin-shell condition underestimates the fifth force especially with $R_{\rm env} = 5\,h^{-1}$ Mpc. This is probably because the chameleon mechanism becomes weaker for larger $|f_{R0}|$, and the environmental effect becomes more non-local. Thus we need a larger $R_{\rm env}$ to capture the environmental effect correctly.

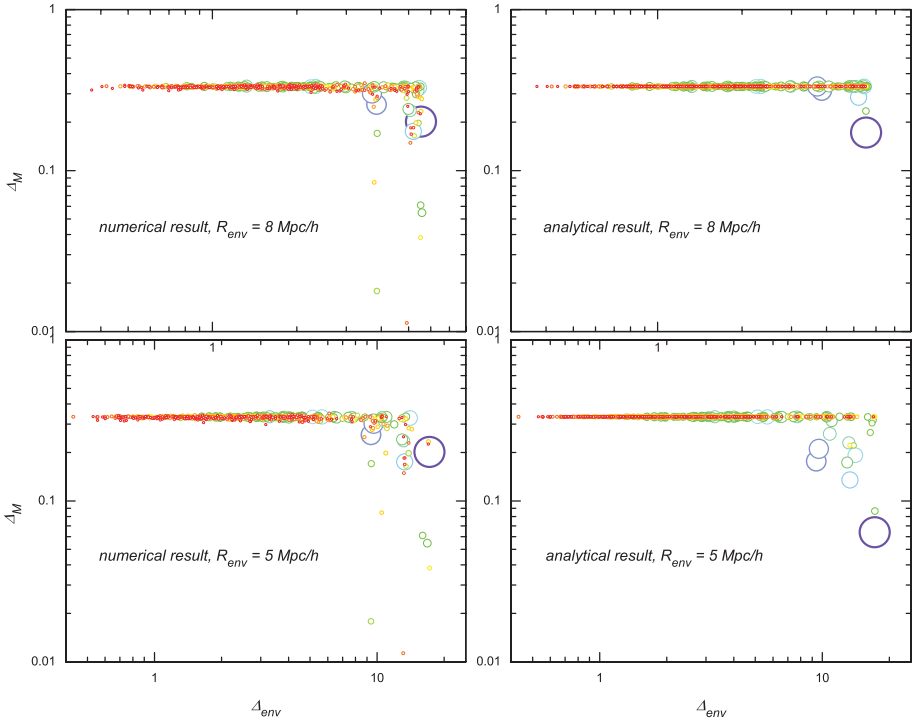

Figure 3. The same as Fig. 2, but for the model with $|f_{R0}| = 10^{-5}$.

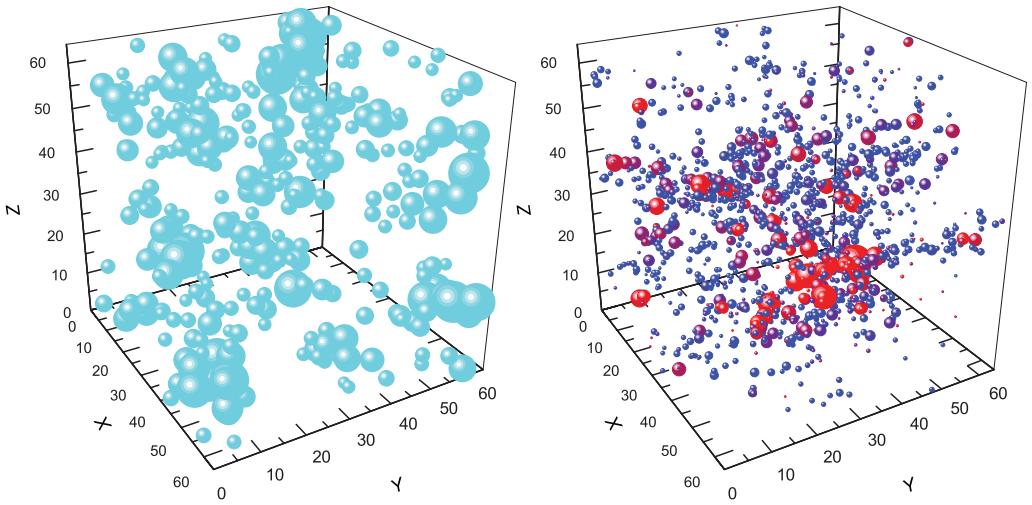

Figure 4. A visualization of the distributions of voids and dark matter haloes in one of our $|f_{R0}| = 10^{-6}$ simulations. Each bubble represents a protovoid (left-hand panel, where the bubble size characterizes the size of the protovoid) and halo (right-hand panel, where the bubble size characterizes the halo's mass). The colour of a halo represents the screening of that halo, from strongly screened (red) to unscreened (blue).

Another possible reason for the slight discrepancy between analytical and numerical results is that the dark matter haloes are not rigorously spherical, which we have assumed when applying the thin-shell condition; we have tried to search for the possible correlation between the ellipticity of the haloes and Δ_M, but we did not find any evidence, which means that using the spherical thin-shell condition is indeed a good approximation.

5 VOIDS

Next let us turn to the underdense regions, or voids, in the $f(R)$ gravity.

The voids are identified using the VAMSUR (Voids As Merged Spherical Underdense Regions) code developed by Li (2011). The basic idea is to first find the low-density spherical regions (protovoids) and then merge them to form irregularly shaped voids using a given algorithm. In this work we have chosen $\delta < -0.8$ as the definition of voids.

In Fig. 4 we show the protovoids (left-hand panel) and dark matter haloes (right-hand panel) identified in one of our simulation boxes for the model with $|f_{R0}| = 10^{-6}$. We can see the following.

(i) Most dark matter haloes (in particular the more massive ones) distribute in regions where few protovoids can be identified, and vice versa, which is a trivial test of the code and numerical results.

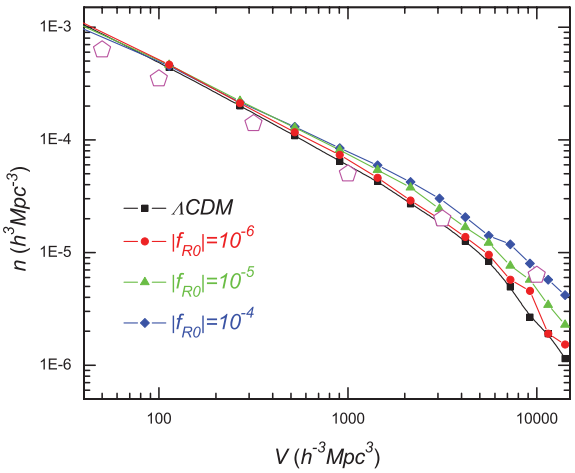

Figure 5. The void number density as a function of volume. The black squares, red circles, green triangles and blue diamonds are from the ΛCDM simulation and $f(R)$ simulations with $|f_{R0}| = 10^{-6}, 10^{-5}, 10^{-4}$. Each curve is the averaged result of 10 realizations. The magenta pentagons are results for ΛCDM from Colberg et al. (2005) for a consistency check [the agreement is reasonable given that we use simulations of different size and resolution, and that the different void finders and void definitions usually lead to very different void measurements (Colberg et al. 2008)]. All results are at $a = 1$.

(ii) Near the voids, the dark matter haloes are less screened (denoted in blue), while far from the voids they can be well screened (in red).

These observations agree with our expectation very well.

As mentioned above, in the $f(R)$ gravity the fifth force helps evacuate the low-density regions, which results in more large voids than in ΛCDM. To see this more clearly, one could plot the number density of voids as a function of their effective volumes, and this is shown in Fig. 5 (see figure caption for details). Here we can see the clear trend: increasing $|f_{R0}|$, which makes the fifth force less suppressed from earlier times, produces more large voids. For example, an $f(R)$ universe with $|f_{R0}| = 10^{-5}$ (10^{-4}) has twice (four times) as many voids with effective radius $15\,h^{-1}$ Mpc as a ΛCDM universe does, and the relative difference in the abundance for larger voids is even larger.

Very large voids and very massive dark matter haloes are rare objects in a ΛCDM universe, and we have seen that both of them are more abundant in the $f(R)$ universes. This is the reason why cluster abundance gives the strongest constraints on $|f_{R0}|$ with current observations (Schmidt, Vikhlinin & Hu 2009; Ferraro, Schmidt & Hu 2011; Lombriser et al. 2011). Compared with the haloes, the modified gravity effect is more pronounced on the voids. This is because in $f(R)$, gravity is maximally enhanced in voids due to the presence of the fifth force. At $z = 0$, the model with $|f_{R0}| = 10^{-5}$ predicts ∼30 per cent more haloes with mass $\sim 5 \times 10^{14}\,\mathrm{M}_{\odot}$ than ΛCDM (Zhao et al. 2011a), while it predicts twice as many voids of size $\sim 15\,000\,h^{-3}\,\mathrm{Mpc}^3$.

Due to the limitation of our simulation box size, we do not have voids with radius larger than $\sim 15\,h^{-1}$ Mpc. However, there is an abundance of such large voids observed. For example, using the Sloan Digital Sky Survey Data Release 7, Pan et al. (2011) identified about 1000 voids in the Northern Galactic hemisphere with radii $> 10\,h^{-1}$ Mpc; the largest and median radii in their void catalogue are 30 and $17\,h^{-1}$ Mpc, respectively. Those voids have an edge density contrast of $\delta < -0.85$. They find that their observations agree quite well with the ΛCDM simulations, which means that their data could place strong constraints on the $f(R)$ gravity, making voids a promising tool to study the physics of the accelerated cosmic expansion and large-scale structure formation. Of course, their voids are identified by looking at galaxies in the survey, and to make direct comparison with their data we have to generate galaxy catalogues in the $f(R)$ gravity. We will leave this to future work.

6 SUMMARY AND CONCLUSIONS

In this paper, we studied the overdense and underdense regions, namely the distribution of haloes and voids, in $f(R)$ gravity simulations. By comparing the probability distribution function of the density contrast δ for $f(R)$ models with that for GR, we find that there are far more voids in $f(R)$ gravity than that in GR. For example, the numbers of voids with an effective radius of $15\,h^{-1}$ Mpc are twice and four times as many as those in GR for $f(R)$ models with $|f_{R0}| = 10^{-5}$ and 10^{-4}, respectively. This in principle provides a new means to test GR observationally using the upcoming data. We also find that haloes near the voids are less screened and experience stronger gravity. Especially, haloes inside the voids are significantly less screened in our simulations. This confirms the expectations that small galaxies inside voids provide us with the best place for testing modification of gravity.

On the other hand, the overdense regions, i.e. the distribution of dark matter haloes, can provide important information for the GR test as well. In this work, we utilized the thin-shell condition developed in Khoury & Weltman (2004) and Li & Efstathiou (2011), and analytically predicted the fractional difference between the lensing mass and the dynamical mass of dark matter haloes, Δ_M, as a function of the environment. As we found, the analytic result agrees very well with the simulation result, which means that the thin-shell condition is a good approximation for $f(R)$ gravity. This has important applications for the semi-analytic halo model building for $f(R)$ gravity, which is crucial for realistic constraints of $f(R)$ models using observations.

ACKNOWLEDGMENTS

BL is supported by the Royal Astronomical Society, Queens' College and the Department of Applied Mathematics and Theoretical Physics of the University of Cambridge, and thanks the Institute of Cosmology and Gravitation of the University of Portsmouth for hosting him when part of this work was done. G-BZ and KK are supported by STFC grant ST/H002774/1. KK acknowledges supports from the European Research Council and the Leverhulme Trust.

REFERENCES

Brax P., van de Bruck C., Davis A. C., Shaw D. J., 2010, Phys. Rev. D, 82, 063519
Brax P., van de Bruck C., Davis A. C., Li B., Shaw D. J., 2011, Phys. Rev. D, 83, 104026
Carroll S. M., de Felice A., Duvvuri V., Easson D. A., Trodden M., Turner M. S., 2005, Phys. Rev. D, 71, 063513
Colberg J. M., Sheth R. K., Diaferio A., Gao L., Yoshida N., 2005, MNRAS, 360, 216
Colberg J. M. et al., 2008, MNRAS, 387, 933
Copeland E. J., Sami M., Tsujikawa S., 2006, Int. J. Modern Phys. D, 15, 1753
Davis A. C., Li B., Mota D. F., Winther H. A., 2011, ApJ, in press (arXiv:1108.3082)
Ferraro S., Schmidt F., Hu W., 2011, Phys. Rev. D, 83, 063503
Hellwing W. A., Juszkiewicz R., 2009, Phys. Rev. D, 80, 083522

Hinterbichler K., Khoury J., 2010, Phys. Rev. Lett., 104, 231301
Hu W., Sawicki I., 2007, Phys. Rev. D, 76, 064004
Khoury J., Weltman A., 2004, Phys. Rev. D, 69, 044026
Li B., 2011, MNRAS, 411, 2615
Li B., Barrow J. D., 2007, Phys. Rev. D, 75, 084010
Li B., Barrow J. D., 2011, Phys. Rev. D, 83, 024007
Li B., Efstathiou G., 2011, MNRAS, in press (arXiv:1110.6440, doi:10.1111/j.1365-2966.2011.20404.x)
Li B., Zhao H., 2009, Phys. Rev. D, 80, 044027
Li B., Zhao H., 2010, Phys. Rev. D, 81, 104047
Li B., Zhao G., Teyssier R., Koyama K., 2012, J. Cosmol. Astropart. Phys., 01, 051
Lombriser L., Slosar A., Seljak U., Hu W., 2011, preprint (arXiv:1003.3009)
Mota D. F., Shaw D. J., 2007, Phys. Rev. D, 75, 063501
Oyaizu H., 2008, Phys. Rev. D, 78, 123523
Oyaizu H., Lima M., Hu W., 2008, Phys. Rev. D, 78, 123524
Pan D. C., Vogeley M. S., Hoyle F., Choi Y. Y., Park C., 2011, preprint (arXiv:1103.4156)
Schmidt F., 2010, Phys. Rev. D, 81, 103002
Schmidt F., Lima M., Oyaizu H., Hu W., 2008, Phys. Rev. D, 79, 083518
Schmidt F., Vikhlinin A., Hu W., 2009, Phys. Rev. D, 80, 083505
Zhao H., Maccio A., Li B., Hoekstra H., Feix M., 2010, ApJ, 712, L179
Zhao G., Li B., Koyama K., 2011, Phys. Rev. D, 83, 044007
Zhao G., Li B., Koyama K., 2011, Phys. Rev. Lett., 107, 071303

This paper has been typeset from a TEX/LATEX file prepared by the author.